Available online at www.sciencedirect.com
ScienceDirect
Journal of Solid State Chemistry 179 (2006) 3883–3892
JOURNAL OF SOLID STATE CHEMISTRY
www.elsevier.com/locate/jssc

Ag_2CuMnO_4: A new silver copper oxide with delafossite structure

David Muñoz-Rojas[a], Gloria Subías[b], Judith Oró-Solé[a], Jordi Fraxedas[a], Benjamín Martínez[a], Montse Casas-Cabanas[a], Jesús Canales-Vázquez[a], Jose Gonzalez-Calbet[d], Ester García-González[d], Richard I. Walton[c], Nieves Casañ-Pastor[a,*]

[a]*Institut de Ciència de Materials de Barcelona, CSIC, Campus U.A.B., Bellaterra, Spain*
[b]*Instituto de Ciencia de Materiales de Aragón, CSIC-Universidad de Zaragoza Pza. San Francisco s/n, 50009—Zaragoza, Spain*
[c]*Department of Chemistry, University of Warwick, Coventry CV4 7AL, UK*
[d]*UCM, Departamento de Química Inorgánica, Facultad de Químicas, Universidad Complutense, 28040 Madrid, Spain*

Received 17 June 2006; received in revised form 17 August 2006; accepted 21 August 2006
Available online 24 August 2006

Abstract

The use of hydrothermal methods has allowed the synthesis of a new silver copper mixed oxide, Ag_2CuMnO_4, the first example of a quaternary oxide containing both elements. It crystallizes with the delafossite 3*R* structure, thus being the first delafossite to contain both Ag and Cu. Synthesis conditions affect the final particle size (30–500 nm). Powder X-ray diffraction Rietveld refinement indicates a trigonal structure $(R\bar{3}m)$ and cell parameters $a = 2.99991$ Å and $c = 18.428$ Å, where Cu and Mn are disordered within the octahedral B positions in the plane and linearly coordinated Ag occupies de A position between layers. X-ray absorption near edge spectroscopy (XANES) for copper and manganese, and XPS for silver evidence +2, +4, and +1 oxidation states. The microstructure consists of layered particles that may form large twins showing 5 nm nanodomains. Finally, magnetic measurements reveal the existence of ferromagnetic coupling yielding in-plane moments that align antiferromagnetically at lower temperatures. The singularity of the new phase resides on the fact that is an example of a bidimensional arrangement of silver and copper in an oxide that also shows clear bidimensionality in its physical properties. That is of special relevance to the field of high T_c superconducting oxides, while the ferromagnetic coupling in a bidimensional system deserves itself special attention.

Keywords: Silver; Copper; Manganese; Mixed oxides; Delafossite structure; Hydrothermal synthesis; Soft chemistry; Anisotropy; Ferromagnetism and antiferromagnetism

1. Introduction

The search for layered cuprates has been profoundly enhanced by the observation of high T_c superconductivity. Among them, the oxides containing mercury have shown the highest T_c values. However, the chemistry of mercury and its toxicity has promoted the search of analogues with metals of similar coordination, which are not many. In particular silver is the closest one and the effort has been focused not always successfully to the copper–silver combination. These oxides are surprisingly absent in nature despite the natural existence of sulfides and selenides. Very recently several new oxides containing silver and copper have been synthesized by the use of unusual soft chemistry procedures. $Ag_2Cu_2O_3$ and $Ag_2Cu_2O_4$, [1–4] are the simplest and most representative phases in a family that also includes a solid solution, $Ag_5Pb_{2-x}Cu_xO_6$ [5] ($0 \leqslant x \leqslant 0.5$) and an oxygen overstoichiometric phase $Ag_2Cu_2O_{4.33}$ [6]. In the case of $Ag_2Cu_2O_3$, an acid–base co-precipitation synthesis procedure followed by aging was used. Both chemical [4] and electrochemical [2,3] oxidation procedures yielded simultaneously in two different laboratories $Ag_2Cu_2O_4$, a phase whose electronic structure has very unique features [7]. Oxidized silver and copper can be found in this phase with unusual charge distributions that also involve oxygen. Electrochemical methods allow the

*Corresponding author. Fax: +34 93 5805729.
E-mail address: nieves@icmab.es (N. Casañ-Pastor).

0022-4596/$ - see front matter © 2006 Elsevier Inc. All rights reserved.
doi:10.1016/j.jssc.2006.08.020

synthesis of better crystallized samples, solid state transformations among $Ag_2Cu_2O_3$ and $Ag_2Cu_2O_4$ phases are also possible, [8,9] and ozonization probed the possible existence of over-stoichiometric oxygen that could be dissolved in the structure [6].

On the other hand, typical delafossites contain either Ag^I or Cu^I [10,11] (Cu^{II} being also found in the B layer [12]), while to the best of our knowledge, there are no reports of delafossites containing both metals. Even though the recently discovered $Ag_2Cu_2O_4$ presents the same stoichiometry and metals than typical delafossites, it crystallizes in the monoclinic system, with the space group $C2/m$, due to a high degree of distortion of the octahedra in the Cu layer [2–4]. It is very similar indeed to what happens when dealing with Cu and Mn. In crednerite, $CuMnO_2$, the Jahn–Teller distortion associated to Mn^{III} eliminates the $R\bar{3}m$ symmetry associated to delafossite crystallizing again with the space group $C2/m$ (monoclinic system), and thus no Cu/Mn true delafossite is yet known [10,11]. Only the introduction of another metal, i.e. Sb [13], in the B layer yields a delafossite structure. In this case, a formal exchange of half of the Cu in $Ag_2Cu_2O_4$ for Mn has produced the same effect, yielding the first Ag/Cu known delafossite structure.

This paper shows the synthesis of a new mixed silver copper oxide with a delafossite structure, Ag_2CuMnO_4, using very soft hydrothermal methods in oxidizing conditions. The hydrothermal decomposition of the oxidant, $KMnO_4$, creates a layered arrangement that the new phase emulates, and that may be the mechanism of its formation. Hydrothermal syntheses have already been known as very useful low-temperature methods for the preparation of complex oxides, [10,14] although when silver is involved it tends to get reduced to metallic Ag^0. In this case, the synthesis of a new oxide in the family of silver–copper oxides is achieved in the very low temperature range of the method under strong oxidizing conditions. The new phase Ag_2CuMnO_4, reported for the first time in this paper, is a magnetic delafossite that shows rather unusual small particle size, structural and magnetic properties. All those aspects may be of high interest in fundamental and applied physics in the near future, as this phase combines ferro- and antiferromagnetic interactions within a very small spatial range, and bidimensional arrangement. Additionally, the formation of a specific structural type based on the permanganate decomposition reaction can certainly be very attractive from a fundamental point of view. Furthermore we are dealing with the first truly bidimensional cuprate containing linear silver joining the copper layers, a fact that brings us closer to the structural features found in high T_c superconductors.

2. Experimental

2.1. Synthesis

All reactions were carried out in hydrothermal conditions. The phases reported have been prepared at 120 °C from mixtures of AgO (Aldrich), $CuSO_4$ (PROBUS) and $KMnO_4$ (Panreac p.a.) as starting materials. In a typical synthesis, 0.10 g of AgO, 0.08 g of $CuSO_4$ and 0.09 g of $KMnO_4$ were mixed in 12 ml of distilled water an stirred vigorously up to 45 min. Afterwards, 0.93 g of NaOH were added to the suspension and stirred for 1 min. The suspension was then transferred to a 23 ml Teflon™-lined autoclave (Parr-Bomb) and heated at 1 °C/min up to 120 °C, temperature that was maintained for 10 h. After natural cooling, the so-obtained precipitate was filtered, washed and dried at 50 °C, rendering a black solid. The products of this same reaction when the Ag precursor or Cu precursor were alternatively supressed were, respectively, CuO and Ag_2O. Indeed, the reaction product is remarkably sensitive to the different variables and conditions. It could be obtained at temperatures below 100 °C only when using a close vessel, hence assuring some degree of overpressure. On the other hand, a temperature increase or a large reaction time favored phase amorphization. The use of alternative metallic precursors to the aforementioned, i.e. $AgSO_4$, $AgNO_3$ or MnO_2 among others, did not yield any traces of Ag_2CuMnO_4.

In other cases, the amount of permanganate excess, heating rate or stirring time caused variations in the microstructure. Thus, the use of large excess of $KMnO_4$, together with a decrease in the stirring time prior to the reaction, yielded a dark-brown precipitate that consisted of Ag_2CuMnO_4 with a smaller particle size along with an amorphous impurity derived from $KMnO_4$ decomposition. (Hydrothermal treatment of $KMnO_4$ alone in the same conditions yielded a brown solid which has a disordered layered structure highly related to that of Birnesite [15]. Permanganate reduction occurs spontaneously in water in alkaline conditions and seems to be accelerated by temperature and hydrothermal conditions, the reducing agent being water). Bulk analysis were performed by ICP atomic absorption in all samples with an estimated error of 10% on average. TGA analysis were performed on a Perkin-Elmer TA 7 system in oxygen, and show that the phases are stable up to 500 °C.

Although we will mainly focus in the analysis of the product of the first synthesis described (hereafter Ag_2CuMnO_4-L), which yields the largest particle size, the results for the smaller sample ($AgCuMnO_4$-S) will also be introduced when suitable, for comparative purposes.

2.2. Characterization: x-ray diffraction

Powder X-ray diffraction patterns (XRD) were collected using a rotating anode Rigaku Rotaflex Ru-200B diffractometer with Cu$K\alpha$ radiation ($\lambda_1 = 1.5060$ and $\lambda_2 = 1.5444$ Å) in the angular range $5 \leqslant 2\theta \leqslant 90°$, with a step size of 0.02° and at a scanning rate of 0.16°/min. Rietveld refinement was performed with the FullProf program [16,17] using the Thompson, Cox and Hastings Pseudo-Voigt profile function [18]. The parameters constituting the instrumental resolution function (U, V, W) used in the Rietveld refinement were obtained from a

quartz standard ($U = 0.031086$, $V = -0.039128$ and $W = 0.021653$) although U was lead to vary in order to account for isotropic strains. Anisotropic size broadening due to the small size and the anisotropic shape of the coherent domains was modeled as a linear combination of Spherical Harmonics [19,20].

2.3. Electron microscopy

Morphological characterization of the sample was carried out using a Phillips XL-30 field-emission gun (FEG) scanning electron microscope. Transmission electron microscopy (TEM) and selected area electron diffraction studies were performed on a JEOL 1210 transmission electron microscope operating at 120 kV and equipped with a side-entry $\pm 60^\circ/\pm 30^\circ$ double tilt. High-resolution images were obtained with two microscopes: a JEOL JEM 2011 electron microscope equipped with a ($\pm 20^\circ$) double-tilt sample holder, operating at 200 kV and fitted with an Oxford Link detector to perform EDS analysis, and a JEOL 4000EX operating at 400 kV. Samples for TEM work were prepared by dispersion of fine ground material onto a perforated carbon film supported on a Cu or Al grid.

EDS analyses performed with the different microscopes statistically over a large number of particles and agglomerates of Ag_2CuMnO_4-L shows the presence of the three elements in each analyzed crystal and confirms the stoichiometry of the sample (also confirmed by atomic absorption analyses). $Ag_2Cu_2O_3$ [1] and $CnMnO_2$, synthesised as in Ref [21], were used as standards for EDS quantification.

2.4. X-ray absorption spectroscopy (XAS)

Measurements were performed on Station 7.1 of the Daresbury SRS at the manganese and copper K-edges. The SRS operates with an average stored-energy of 2 GeV and a typical electron-current of 200 mA and Station 7.1 receives X-rays in the 4–10 keV energy range. The station is equipped with a harmonic-rejecting, double-crystal Si(111) monochromator, with its second crystal allowing sagittal focusing of the X-ray beam. Harmonic rejection was set to 50% for all experiments, by detuning the second crystal to 50% of the maximum X-ray intensity. Data were collected in transmission mode from pellets prepared by pressing powdered sample materials diluted, when necessary, with polyethylene powder (spectrophotometric grade, Aldrich). Dilution was required to prevent self-absorption (values for the full absorption and edge jump of, $\mu d = 2.5$, and $\Delta\mu d \approx 1$ were used). Ionization chambers placed before (I_0) and behind (I_t) the sample were filled with appropriate quantities of inert gases (Ar–He mixture) to maximize the detection of the X-rays. On Station 7.1, data were also measured simultaneously from a 5 μm metal foil (of the element whose edge was studied) placed between the second and a third (I_m) ionization chamber to provide an edge-shift calibration for the XANES data. Copper and manganese foils were used as reference for energy calibration. Data were collected in two regions: (1) the pre-edge region with a step size equivalent to 10 eV to allow a pre-edge background calculation and subtraction, and (2) the XANES region from 30 eV below the edge to 50 eV above the absorption edge, with a step size equivalent to ~0.2 eV. The data were analyzed using the Daresbury Laboratory suite of software. [22] The program EXCALIB was used to normalize all data and EXBROOK was used to produce normalized XANES spectra by the edge step method and by positioning the E_0 value using the maximum in the first derivative, recalibrating the spectrum around this value, then subtracting the pre-edge background using a quadratic fit.

2.5. XPS analysis

XPS measurements were performed at room temperature with a SPECS EA10P hemispherical analyzer using both non-monochromatic Mg $K\alpha$ radiation (1253.6 eV) as excitation source in a base pressure of $\approx 10^{-9}$ mbar, on pressed pellets, avoiding to use silver epoxy.

2.6. Magnetism

Magnetic data were obtained using a SQUID magnetometer at 10,000 Gauss and also at 10 Gauss under ZFC-FC conditions. A hysteresis loop at liquid helium was measured between ±10,000 Gauss that showed no hysteresis.

3. Results and discussion

Fig. 1 shows the X-ray diffraction patterns for samples Ag_2CuMnO_4-L and Ag_2CuMnO_4-S, obtained after hydrothermal reaction in different conditions, as detailed above.

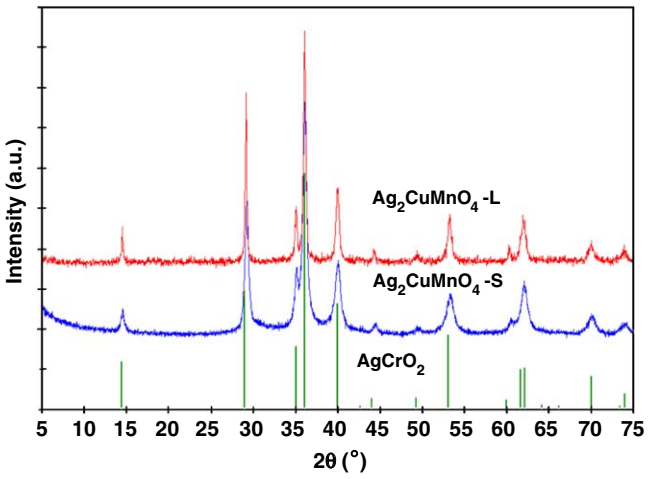

Fig. 1. Powder X-ray diffractograms for Ag_2CuMnO_4-S and Ag_2CuMnO_4-S. Diffraction lines corresponding to AgCrO2 (ICSD CC# 4149) are also indicated.

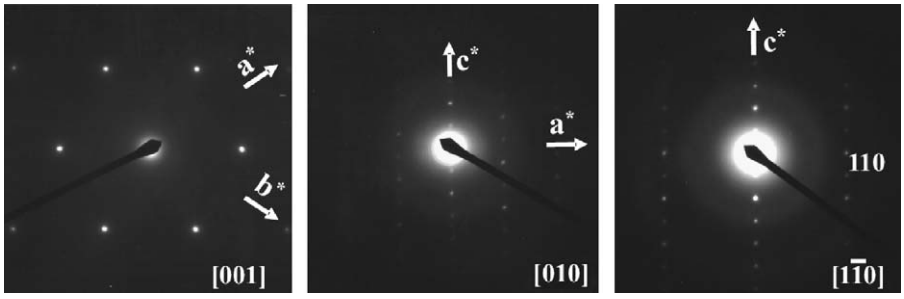

Fig. 2. SAED images of Ag_2CuMnO_4-L showing base planes [001], [010] and [1$\bar{1}$0].

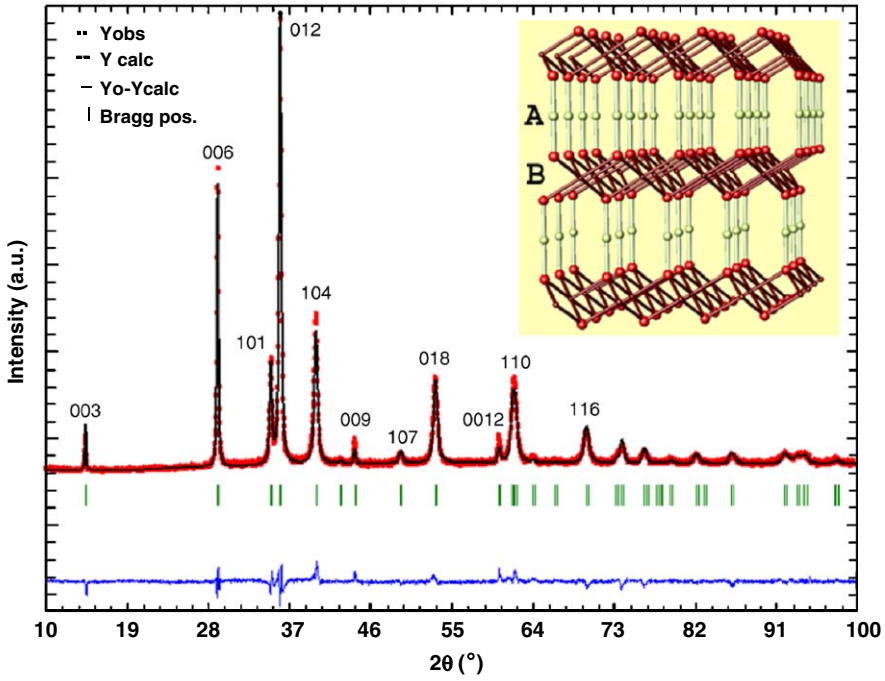

Fig. 3. X-ray Rietveld refinement of Ag_2CuMnO_4-L. Inset: Resulting delafossite structure.

As can be appreciated, the powder pattern corresponding to Ag_2CuMnO_4-L presents narrower peaks, indicating larger and better crystallized particles than in the case of Ag_2CuMnO_4-S. Thus, experimental synthesis conditions are determinant in the final particle size.

The X-ray powder diffraction pattern of Ag_2CuMnO_4 is characteristic of a delafossite-type structure ($A^IB^{III}O_2$, see inset in Fig. 3), almost identical to that of the delafossite $AgCrO_2$ [23,24] (Fig. 1), which crystallizes in the $R\bar{3}m$ space group. Reconstruction of the unit cell from selected area electron diffraction (SAED) patterns performed on Ag_2CuMnO_4 yielded an hexagonal unit cell that could be indexed with the $R\bar{3}m$ space group. Fig. 2 shows the [100], [010] and [1$\bar{1}$0] base planes. The measured cell parameters, $a = 3.0$ Å and $c = 18.5$ Å, are also rather close to those of $AgCrO_2$ ($a = 2.985$ Å and $c = 18.51$ Å).

Accordingly, Rietveld refinement was performed for Ag_2CuMnO_4 taking as initial parameters those of the delafossite $AgCrO_2$ [24]. Since the X-ray scattering factors for Mn and Cu are very similar, a random distribution of these metals in B positions was assumed in the refinement.

Fig. 3 shows the agreement between the calculated and observed profiles for Ag_2CuMnO_4-L. The parameters for the instrumental resolution function (U, V, W)$_{instr}$. were obtained from a quartz standard as detailed above, although an additional U_{sample} was also refined in order to allow for an isotropic strain in the microstructural refinement. After the preliminary refinements performed to fit the scale factor, zero point displacement and cell parameters, several cycles were performed to refine the spherical harmonics coefficients, atomic positions, isotropic strains and finally isotropic thermal displacements. The results of the refinement are listed in Table 1 together with the final agreement factors. Distances and angles are shown in Table 2.

According to these results, Ag_2CuMnO_4 crystallizes with delafossite structure with both, Cu and Mn, located in the corresponding B octahedral position, sharing edges among them. The refinement yields averaged distorted oxygen octahedra for the metals in the B-site with average M–O distances $\approx 1.937(2)$ Å (see Table 2), according to the symmetry associated to the space group $R\bar{3}m$. As in many

Table 1
Refinement parameters for the large particle phase Ag_2CuMnO_4-L

Space group	$R\bar{3}m$
Unit cell	$a = 2.9938(2)$ Å
	$b = 2.9938(2)$ Å
	$c = 18.441(2)$ Å
Cell volume	143.142(7) Å^3
Density	6.929 g/cm^3
Z	3
Points	3001
Effective 2θ	10–100
Refined parameters	24 (background points included)
R_B; R_F, R_{exp}	5.27, 4.7, 4.17
χ^2	2.63

Atom	x	y	z	Biso
Ag	0	0	0	1.8(2)
Cu/Mn	0	0	0.5	0.6(2)
O	0	0	0.8807(9)	2.3(5)

Table 2
Distances and angles obtained from X-ray refinement

Bond	Distance (Å)
Ag–O	2.200(6)
Ag–Ag	2.9938(2)
Ag–Cu/Mn	3.5262(9)
Cu/Mn–Cu/Mn	2.9938(2)
Cu/Mn–O	1.937(2)
Angle	**Degrees**
O–Ag–O	180.0(2)
O–Cu/Mn–O	78.8(1), 101.2(1)
Cu/Mn–O–Ag	116.8(2)
Cu/Mn–O–Cu/Mn	85.9(1)

other delafossites, the A site is occupied by linearly-coordinated Ag^I [10,11], with an Ag–O distance of 2.200(6) Å. This value is larger than the corresponding to other silver delafossite structures or silver oxides. Those values range from 2.04 Å in Ag_2O to 2.25 Å in $Ag_2Cu_2O_4$ and summarized in Ref. [7]. However, it has to be kept in mind that X-ray diffraction is yielding an average structure, and therefore no conclusion can be drawn from that value. The single crystallographic oxygen is coordinated to the three metals in the structure, in a high symmetry space group where two of the metals, Cu and Mn, have almost identical scattering factors, and as the oxygen position is the result of the different coordination for Cu and Mn, a substantial influence is expected also for the Ag–O distance.

Preliminary neutron diffraction experiments do not show any Cu/Mn ordering (see Supplementary material). Furthermore, SAED images (see Fig. 2) do not show any superstructure as expected for a lowering in symmetry related with differences in coordination.

Partial occupancy and sub-stoichiometries were attempted in the X-ray refinement, with no success. An excess electron density is found by difference Fourier mapping at the heaviest element, Ag, that could lead to a 90% silver amount with respect to the stoichiometric. However, disorder and averaged structure may be compensated in such an effect and that was not taken as indicative, as both chemical and EDS analysis show otherwise.

A similar refinement can be carried out for Ag_2CuMnO_4-S, yielding very slight variations of cell parameters and distances, and showing no evidence of any additional crystalline phase.

In agreement with the refinement stoichiometry, Ag_2CuMnO_4-L atomic absorption analysis shows a 1/0.52/0.47 (Ag/Cu/Mn) ratio with an experimental error of ± 0.05 in the molar ratio. However, in the case of Ag_2CuMnO_4-S, ICP analyses reveal a larger manganese content, namely, a 1/0.5/0.7 ratio, despite that they showed the same diffraction pattern. This can be explained by the presence of an amorphous by-product, probably related with the hydrothermal decomposition of the $KMnO_4$ excess, which would be part of the baseline in the X-ray diffraction pattern. Given the similar structural features of some of the permanganate decomposition products (see discussion below) it is also possible that in these small particles, any broad peak will show up broadening some of the Ag_2CuMnO_4-S diffraction peaks.

Within the polytypes found in delafossites ($2H$ and $3R$), the structure of the quaternary oxide corresponds to $3R$ ($R\bar{3}m$ space group). This is equivalent to three unit formulas (three times the standard B-layer spacing along c) per unit cell with the A layer oriented in the same direction but offset in a three layer sequence, as opposed to the two units found in the $2H$ polytypes. Using a close-packing description and using the same nomenclature than in reference [15] the stacking would be described as: $AbCc'CaBb'BcAa''$ sequence (A, B, C representing the positions of oxygen atoms, a, b, c, the positions of Cu/Mn ions and a', b', c' those of Ag), sequence which corresponds to a $3R$- polytype where adjacent layers are shifted with respect to each other by $-a/3$ along the **a**-axis.

As in this case, Ag_2CuMnO_4, there are many examples of delafossite structures where the B-site is shared by two elements [13,25–29], with the A-site occupied by a +1 ion. Given the average B-site nominal charge must be +3, the combination of valence and stoichiometry of the metals within the B layer must be balanced. Several combinations are indeed theoretically possible: a 1:1 mixture of +2/+4 or +1/+5 cations (no example known), a 2:1 mixture of +2/+5 cations and also a mixture of +3 cations [13]. In our case, and given the metals involved, the expected oxidation states are Cu^{II} and Ag^I, which would imply Mn^{IV}, yielding the formula, $Ag^I_2Cu^{II}Mn^{IV}O_4$. Other combinations, as Cu^{III} and Mn^{III}, cannot be neglected on the basis of the average structure that results form the refinement, that renders the same coordination scheme for

both Cu and Mn and prevents bond valence analysis to yield meaningful values.

Consequently, near edge X-ray absorption spectroscopy (XANES) studies on Ag_2CuMnO_4 were performed at the Cu–K and Mn–K edges to elucidate experimentally the oxidation states of the *B*-site metals. The results of XANES experiments for Cu and Mn are shown in Fig. 4.

Fig. 4 shows the Cu–K edge and Mn–K-edge XANES data for Ag_2CuMnO_4 along with some reference materials: CuO, $Ag_2Cu_2O_3$ and $NaCuO_2$ for Cu, and MnO_2 and Mn_2O_3 for Mn. Cu–K edge XANES has been widely used to study copper oxidation-state, in particular to distinguish between Cu^{I} and Cu^{II}. [30,31] The Cu^{II} XANES spectra show several characteristic absorption features: (i) a weak pre-peak (P) at about 8978 eV associated to the dipole forbidden 1*s*–3*d* transition; (ii) a shoulder (B) at the low-energy part of the main absorption line and (iii) the main resonance (A) at the absorption edge. Both, the shoulder and the main peak are attributed to the dipole 1*s*–4*p* transition. The main absorption line lies at the same energy (~8989 eV) for CuO, $Ag_2Cu_2O_3$ and Ag_2CuMnO_4 whereas it is shifted by 3 eV for $NaCuO_2$. The low-energy shoulder is not present for Ag_2CuMnO_4 as it occurs for non-regular octahedral compounds. Its intensity has been shown to be linked to the tetragonal distortion of the octahedron, increasing by changing from distorted octahedral coordination to perfectly square planar coordination, [32–34]. The Cu–K edge XANES data from Ag_2CuMnO_4 (Fig. 4 Top) therefore confirm the presence of Cu^{II} while the absence of the low-energy shoulder seems to suggest that copper, as expected for Cu^{II}, it is coordinated by distorted oxygen octahedra.

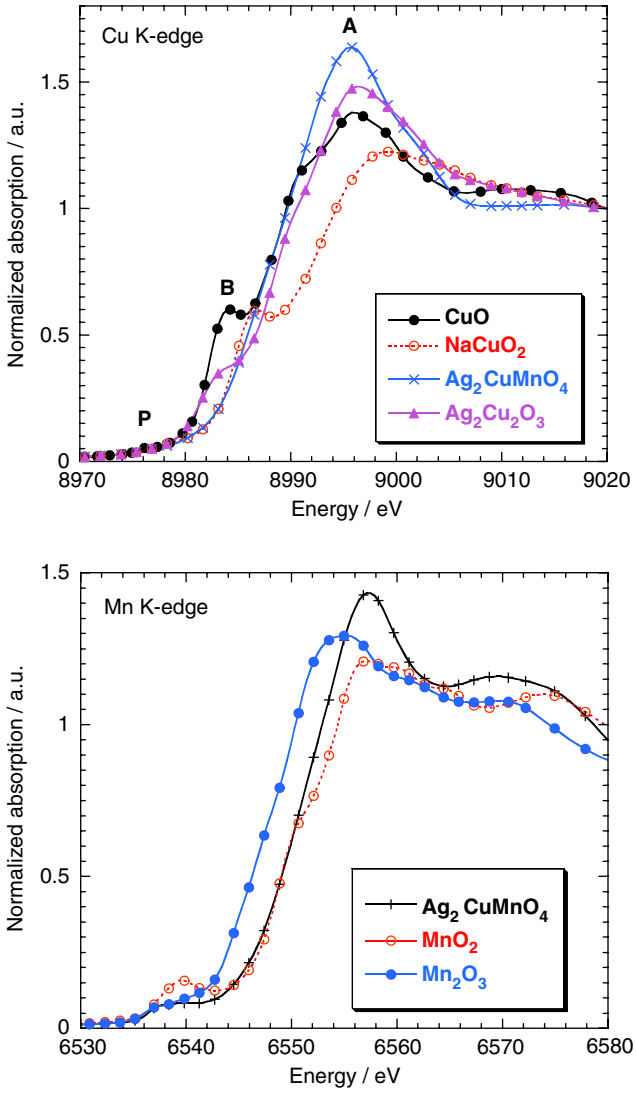

Fig. 4. Top: Cu K-edge XANES data from Ag_2CuMnO_4-S, CuO, $NaCuO_2$ and $Ag_2Cu_2O_3$. Bottom: Mn K-edge XANES for Ag_2CuMnO_4, MnO_2 and Mn_2O_3.

On the other hand, Fig. 4 (Bottom) shows the XANES spectra of Ag_2CuMnO_4 at the Mn–K edge compared to those of Mn_2O_3 and MnO_2 oxides that can be taken as references for formal Mn^{III} and Mn^{IV} oxidation states, respectively. A chemical shift of about 4 eV is observed between the two reference binary oxides in agreement with reported data [35–37]. It is clear from Fig. 4 that Mn in Ag_2CuMnO_4 is in an oxidation state Mn^{IV}. Thereby, the oxidation state assumed for both B cations, Cu^{II} and Mn^{IV}, has been experimentally confirmed, involving Ag^{I}.

The Ag^{I} formal oxidation state of Ag is experimentally confirmed by the XPS data shown in Figs. 5A and B (Ag3*d* and Auger MVV lines, respectively). The energy position and shape of the Ag3$d_{5/2}$ feature (368.5 eV) together with the pronounced valley around 900 eV of the MVV structure are characteristic of Ag^{I}. The Full Widh at Half Maximum (FWHM) of the Ag3$d_{5/2}$ line (1.2 eV) has been also found in other Ag^{I} oxides and denotes the presence of a single silver component [7]. The XPS spectrum of the Cu2*p* region, shown in Fig. 5C, is characteristic of Cu^{II} because of the existence of satellites at ca. 9 eV above the Cu2$p_{3/2}$ (934.2 eV) and Cu2$p_{1/2}$ (954.3 eV) lines. The presence of such satellites is due to the opening of the *d*-shell (d^9). A detailed discussion on this point can be found in Ref. [7]. However, the information extracted from the XPS Mn2*p* lines (see Fig. 5D) is less conclusive than in the case of XANES. The binding energy of the Mn2$p_{3/2}$ line (642.4 eV) is compatible with a formal oxidation state IV, as found for MnO_2 in different data bases [38]. However, similar energies are found for Mn^{II}, so a study based only on XPS would require the comparison of different stable compounds with Mn in different oxidation states under the same experimental conditions. The combination of XPS and XANES on the other hand is sufficient to assure the Mn^{IV} state.

Disorder of Cu and Mn within the B layer may seem unusual based on different coordination preferences for both metals, but in fact it is likely to occur. No ordering of *B* cations in $Ag^{I}_2B^{II}B^{IV}O_4$ delafossites has been ever observed, while in the case of $A^{I}_3B^{II}_2B^{V}O_6$ an ordered arrangement may take place [27–29]. In the case of Ag_2CuMnO_4, a random distribution of *B* cations could help to better accommodate the Jahn–Teller distortion

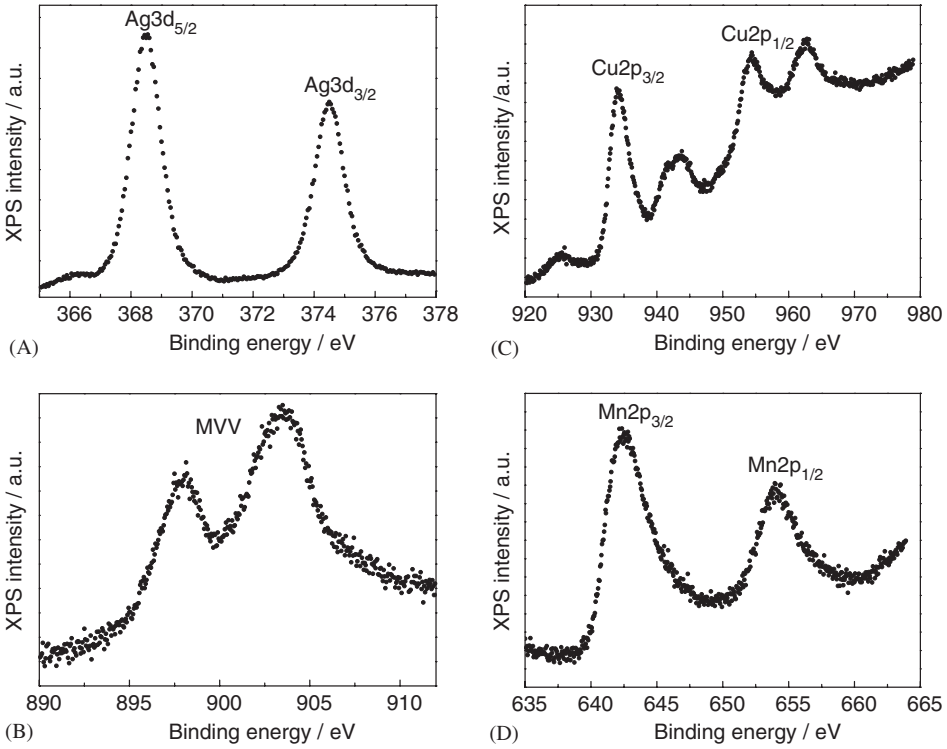

Fig. 5. XPS spectra of: (A) Ag3*d* lines, (B) MVV Auger lines, (C) Cu2*p* lines and (D) Mn2*p* lines.

generally associated to Cu^{II}, as compared with long-range ordering. From another perspective, the delafossite structure may tolerate better such a disorder, as compared with other structural types.

As mentioned above, the formation of the phase in smaller particle size, Ag_2CuMnO_4-S takes place with an impurity that comes from decomposition of excess permanganate. The impurity would most probably be a non-stoichiometric amorphous equivalent of the layered manganese birnessite or ramsdellite, with an approximate formula $K_xMnO_2(H_2O)_y$, which crystallizes in the same space group, $R\bar{3}m$, although with different parameters [24] and hence diffraction angles. In fact K chemical analysis shows the presence of small amounts of this element in a ratio of about 0.1 moles of K per mole of excess manganese observed, which will confirm this impurity. This type of amorphous or quasiamorphous phases, that appear normally as minerals in nature, are hard to synthesize with no faults even when using soft chemistry methods [39] and are usually formed during the hydrothermal alkaline decomposition of $KMnO_4$. They can occlude many types of M(I) and some M(II) ions (Li, H, Na, Ag, Cs, Rb, Ca, Ba) and water molecules between the manganese layers [40,41]. It is also usual that they show quasi-amorphous structures [39].

The high similarity in terms of crystal structure between the main phase in Ag_2CuMnO_4-S and its accompanying impurity suggests that the Ag_2CuMnO_4 oxide may be forming through a mechanism related with the decomposition of permanganate and simultaneous intercalation of cations (especially highly mobile Ag^I). In fact, hydrothermal treatment of permanganate solutions in presence of other transition metals (Co, Ni, Fe) has been used as a synthesis procedure to dope the manganese layer in layered oxides [42], that will be later used as electrodes in lithium batteries, as opposed to exchange reactions [43].

The morphology and microstructure of Ag_2CuMnO_4 has been studied by both SEM and TEM. Ag_2CuMnO_4-L exhibits a high dispersion in morphology and particle size, ranging from 50 up to 500 nm. A calculation from over 40 individual particles yields an average particle size of 177 nm long and 41 nm with. In many cases, twining takes place yielding doughnut-like shaped particles (Fig. 6B), which are usually the largest. The particles tend to agglomerate, which hinders the characterization. Fig. 6A shows a SEM image of one such agglomerate where some of the aforementioned doughnut-like structures can be appreciated. Contrarily to what happens for Ag_2CuMnO_4-L, and as inferred from the XRD patterns, Ag_2CuMnO_4-S shows much smaller particles, i.e. below 40 nm. A smaller dispersion is also observed (Fig. 6C shows a TEM image of some Ag_2CuMnO_4-S crystals for comparison). In this case, twining is not as evident and no instances of doughnut-shaped particles are found. Such morphology is probably an intermediate stadium while particles are still growing and twining to finally yield larger platelet-shaped particles, where an amorphous impurity may have encapsulated the particles preventing further growth.

The microstructure was also evaluated using HRTEM. Fig. 7 shows typical high-resolution images of both Ag_2CuMnO_4-L and Ag_2CuMnO_4-S. In all cases, the measured cell parameters and distances between planes match well the structure refined from XRD data. The

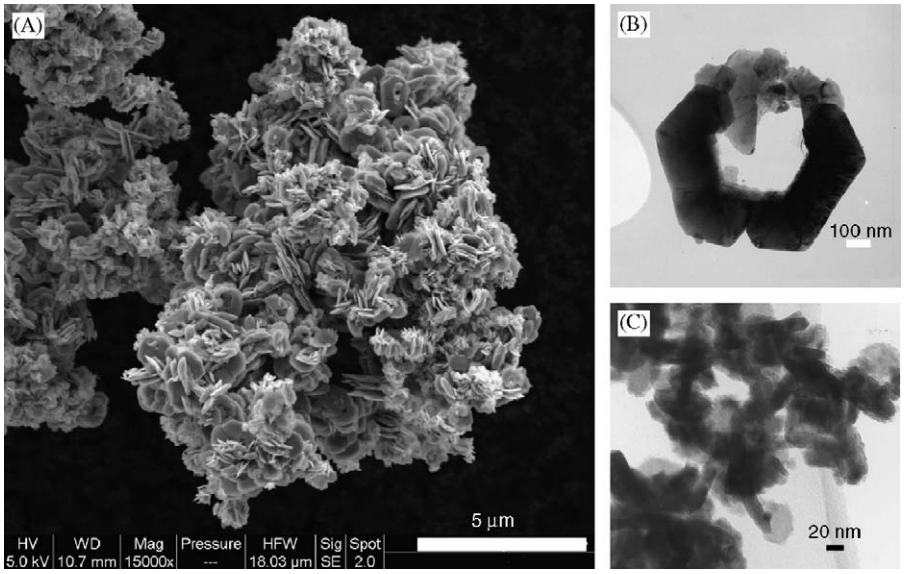

Fig. 6. SEM image corresponding to Ag_2CuMnO_4-L (A). TEM images of Ag_2CuMnO_4-L (B) and Ag_2CuMnO_4-S (C).

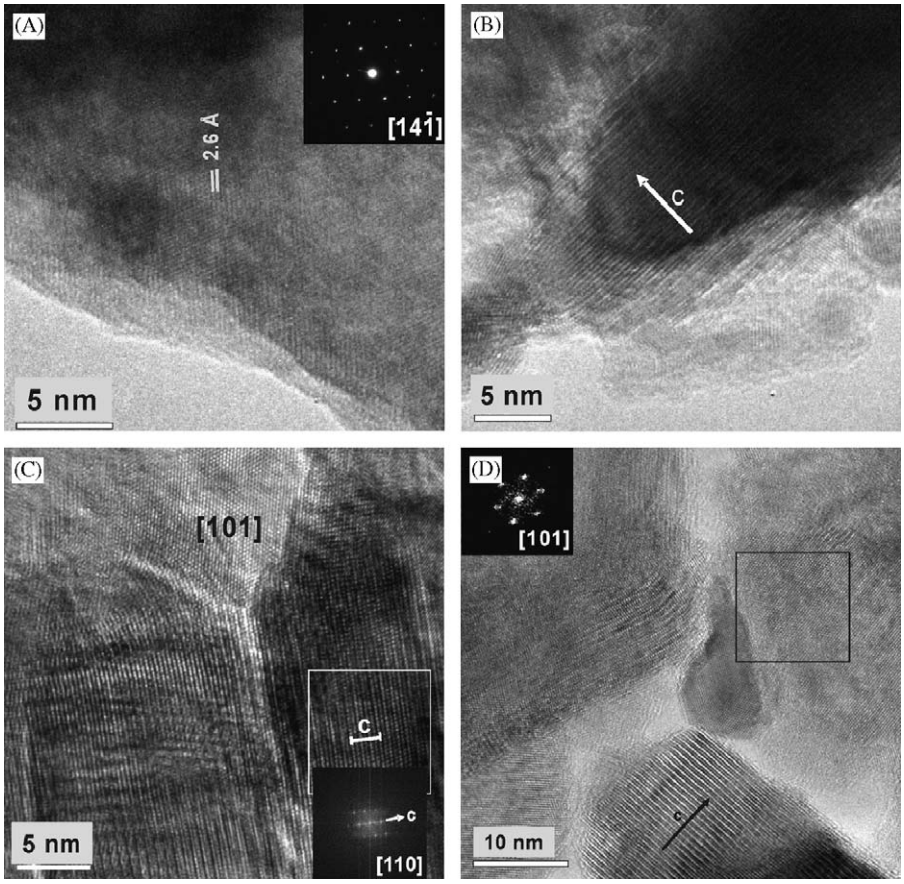

Fig. 7. High resolution transmission electron microscopy images of Ag_2CuMnO_4-L (A, and B, with the corresponding SAED patterns in the inset in case A); and Ag_2CuMnO_4-S (C and D, both showing a Fourier transform of the selected squares).

images show a polycrystalline material constituted by twins of nanosized crystals in random orientations in addition to the existence of nanodomains. Crystallites show preferred orientation down or close to the $[001]_H$ zone axis (sub-index H refers to the corresponding hexagonal cell on the basis of which Miller index are assigned). Some crystals show a characteristic elongated morphology, as shown in Fig. 7B, C and D. In this orientation, it is frequent to observe disorder in the layers packing along the *c* direction. This is common in some delafossite-type phases that may

show different polytypes. A further electron microscopy study is underway for a further evaluation of the nanodomains existing in this and related phases.

The magnetic measurements indicate that both ferromagnetic and antiferromagnetic interactions are present in Ag_2CuMnO_4 in different temperature ranges. The room temperature effective magnetic moment of 3.7 μ_B (Fig. 8 for Ag_2CuMnO_4-L) is consistent with a 50/50 mixture of Cu^{II}–Mn^{IV} (d^9–d^3 ions) each having spin-only moments. This contribution of spin-only values to the magnetic moment is rather usual for both magnetic elements in those oxidation states, Cu^{II} and Mn^{IV} if no coupling occurs. $\chi(T)$ data thus implies that the system is paramagnetic in the higher temperature range. As the temperature decreases, ferromagnetic correlations start to appear below 200 K. Upon further cooling antiferromagnetic correlations show up below approximately 100 K. It is worth mentioning here the absence of hysteresis in $\chi(T)$ curves after zero field cooled/field cooled (ZFC/FC) experiments, therefore strongly suggesting the absence of macroscopic long-range ordering of the magnetic moments.

Taken into account that the layers contain octahedrally coordinated metals sharing edges, with M–O–M distances near 3 Å and containing Cu/Mn–O–Cu/Mn angles (85.9°, see Table 2) near 90°, the results described above can be explained qualitatively according to Goodenough–Kanamori (GK) rules [44,45]. A congruent model may be based on the existence of ferromagnetic interactions working within the Cu/Mn layer planes, between Cu and Mn metals sharing edges, while at lower temperatures antiferromagnetic correlations would appear as a result of interactions between the resulting moments from the planes. These type of interactions, through Ag–O–M bonds of 3.52 Å and Ag–O–M angles near 120° (see Table 2), involve larger distances between magnetic ions and weaker interactions, that can be acting only thanks to the larger size of Ag 4*d* orbitals, and will be expected to work at lower temperatures.

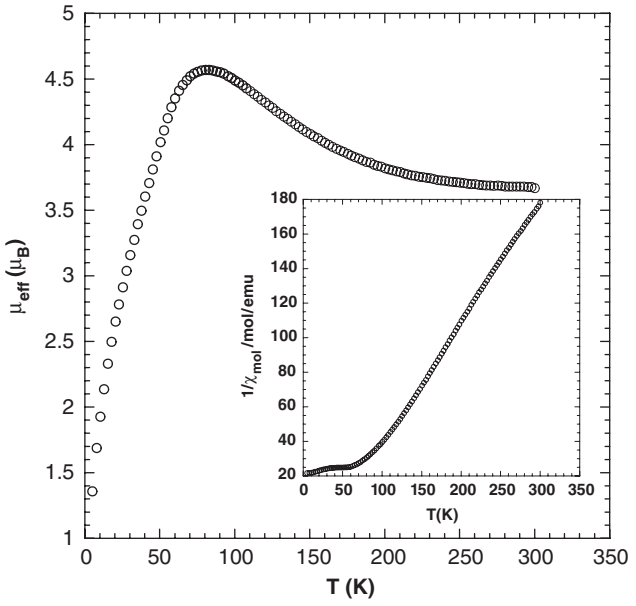

Fig. 8. Effective magnetic moment μ_{eff} (calculated as $(8\chi T)^{1/2}$) vs. T and inverse molar susceptibility, $1/\chi$ vs. T (inset)) for Ag_2CuMnO_4-L. χ refers to molar susceptibility. ($H = 1$ Tesla).

The existence of these two types of interactions does not give a specific clue on any particular crystallographic ordering of Cu/Mn metals, while the lack of hysteresis suggests the absence of long range ordering.

The nanometric phase, Ag_2CuMnO_4-S, shows a magnetic behavior similar to that of Ag_2CuMnO_4-L but with smoother features and larger room temperature effective moment. This last feature is expected, given the presence of an amorphous impurity based on paramagnetic Mn^{IV} ions. The same paramagnetic contribution would add another component to the temperature variation and render smoother ferro and antiferromagnetic transitions. As a whole the magnetic data is internally consistent with the structure and the oxidation states found.

4. Summary

This paper reports a new phase within the recent family of silver-copper mixed oxides, previously unknown, containing silver, copper, and manganese within a layered structure probably related with that found for the hydrothermal decomposition of permanganate. Structure refinements evidence copper and manganese disorder within the planes and silver being coordinated linearly joining planes, and evidence the first delafossite that contains simultaneously silver and copper. Electron microscopy and diffraction assure the existence of a single phase that presents certain disorder in the long range with very small nanodomains in all cases. Magnetic measurements reflect such disorder with the existence of ferromagnetic interactions, most probably between metals within the plane, that do not extend enough to show hysteresis effects. The in- plane moments couple antiferromagnetically upon lowering the temperature. The phase can be prepared in various particle sizes and size distributions and crystallinity. When smaller particle is obtained the phase always comes along with a manganese impurity of the birnessite type that probably is encapsulating the oxide particles and limiting its growth. The larger particle size phase presents better crystallinity and shows a marked tendency to form twins of different types. The implications of such physical properties are under study.

Acknowledgments

The authors thank helpful discussions to P. Gómez Romero and the "Servei de microscòpia de la UAB", and financing from Ministry of Education and Science through grants PB98-0491, MAT2002-04529-C03, MAT 2005-07683-C02-01 a fellowship for DMR and a price from the Fundación Domingo Martínez.

Appendix A. Supplementary materials

Supplementary data associated with this article can be found in the online version at doi:10.1016/j.jssc.2006.08.020

References

[1] P. Gómez-Romero, E.M. Tejada-Rosales, M.R. Palacín, Ang. Chem. Int. Ed. 38 (1999) 524.
[2] D. Muñoz-Rojas, E.M. Tejada-Rosales, P. Gómez-Romero, N. Casañ Pastor, Vth Electroceramics and FIGIPS Meeting in Barcelona, May–June 2001.
[3] D. Muñoz-Rojas, J. Oró, P. Gómez-Romero, J. Fraxedas, N. Casañ-Pastor, Electrochem. Comm. 4 (2002) 684.
[4] J. Curda, W. Klein, H. Liu, M. Jansen, J Alloys Compd. 338 (2002) 99.
[5] E.M. Tejada-Rosales, J. Oró-Solé, P. Gómez-Romero, J. Solid State Chem. 163 (2002) 151.
[6] D. Muñoz-Rojas, J. Fraxedas, P. Gómez-Romero, N. Casañ-Pastor, J. Solid State Chem. 178 (2005) 295.
[7] D. Muñoz-Rojas, G. Subías, J. Fraxedas, P. Gómez-Romero, N. Casañ-Pastor, J. Phys. Chem. B 109 (2005) 6193.
[8] D. Muñoz-Rojas, J. Fraxedas, J. Oró, P. Gómez-Romero, N. Casañ-Pastor, Crys Eng 5 (2003) 459.
[9] D. Muñoz-Rojas, Ph.D. Thesis Dissertation, Universidad Autonoma de Barcelona 2004.
[10] W.C. Sheets, E. Mugnier, A. Barnabé, T.J. Marks, K.R. Poeppelmeier, Chem. Mater. 18 (2006) 7.
[11] M.A. Marquardt, N.A. Ashmore, D.P. Cann, Thin Solid Films 496 (2006) 146.
[12] K. Hayashi, N. Mizutani, M. Kato, Nippon Kagaku Kaishi (1974) 6.
[13] R. Nagarajan, S. Uma, M.K. Jayaraj, J. Tate, A.W. Sleight, Solid State Sci 4 (2002) 787.
[14] R.I. Walton, Chem. Soc. Rev. 31 (2002) 230.
[15] A.C. Gaillot, B. Lanson, V.A. Drits, Chem. Mater. 17 (2005) 2959.
[16] J. Rodríguez-Carvajal, Physica B 192 (1993) 55.
[17] J. Rodríguez-Carvajal, FullProf Program: Multipattern Rietveld, Profile Matching and Integrated Intensity Refinement of X-ray and Neutron Diffraction Data. Version 1.9c May 2001—Laboratoire Leon Brillouin, CEA-CNRS, JRC.
[18] P. Thompson, D.E. Cox, J.B. Hastings, J. Appl. Crystallogr. 20 (1987) 79.
[19] J. Rodríguez-Carvajal, Comission on Powder Diffraction (IUCr) Newsletter 26 (2001) 12.
[20] M. Casas-Cabanas, J. Rodríguez-Carvajal, M.R. Palacín, Powder Diffraction 20 (2005) 334.
[21] M. Trari, J. Töpfer, P. Dordor, J.C. Grenier, M. Pouchard, J.P. Doumerc, J. Solid State Chem. 178 (2005) 2751.
[22] N. Binsted, J.W. Campbell, S.J. Gurman, P.C. Stephenson, EXAFS data analysis program, Daresbury Laboratory, 1991.
[23] $AgCrO_2$: ICSD CC# 4149.
[24] E. Gehle, H. Sabrowsky, Z. Naturf. B, Anorg. Chem. Org. Chem. 30 (1975) 659.
[25] J.P. Doumerc, A. Ammar, A. Wichainchai, M. Pouchard, P. Hagenmuller, J. Phys. Chem. Solids 48 (1987) 37.
[26] Y.J. Shin, J.P. Doumerc, M. Pouchard, P. Hagenmuller, Mater. Res. Bull. 28 (1993) 159.
[27] R. Nagarajan, N. Duan, M.K. Jayaraj, J. Li, K.A. Vanaja, A. Yokochi, A. Draeseke, J. Tate, A.W. Sleight, Int. J. Inorg. Mat. 3 (2001) 265.
[28] M. Marquardt, D. Cann, Mater. Lett. 60 (2006) 81.
[29] K. Ataoui, J.P. Doumerc, A. Ammar, J.C. Grenier, P. Dordor, M. Pouchard, C.R. Chimie, 7 (2004) 29.
[30] L.S. Kau, D.J.S. Solomon, J.E.P. Hahn, K.O. Hodgson, E.I. Solomon, J. Am. Chem. Soc. 109 (1987) 6433.
[31] C. Prestipino, L. Capello, F. D′Acapito, C. Lamberti, Phys. Chem. Chem. Phys. 7 (2005) 1743.
[32] F.W. Lytle, R.B. Greegor, A.J. Panson, Phys. Rev. B 37 (1988) 1550.
[33] J. García, M. Benfatto, C.R. Natoli, A. Bianconi, A. Fontaine, H. Tolentino, Chem. Phys. 132 (1989) 295.
[34] J. Chaboy, A. Muñoz-Paez, F. Carrera, P. Merkling, E. Sánchez-Marcos, Phys. Rev. B 71 (2005) 4208.
[35] G. Subías, J. García, M.G. Proietti, J. Blasco, Phys. Rev. B 56 (1997) 8183.
[36] A.H. De Vries, J. Hozoi, R. Broer, Int. J. Quant. Chem. 91 (2003) 57.
[37] J. Spooren, R.I. Walton, F. Millange, J. Mater. Chem. 15 (2005) 1542.
[38] see e.g., 〈http://srdata.nist.gov/xps/〉
[39] Y. Chabre, J. Pannetier, Prog. Solid St. Chem. 23 (1995) 1.
[40] R. Chen, P. Zavalij, M.S. Whittingham, Chem. Mater. 8 (1996) 1275.
[41] S.L. Brock, N. Duan, Z.R. Tian, O. Giraldo, H. Zhou, S.L. Suib, Chem. Mater. 10 (1998) 2619.
[42] F. Zhang, M.S. Whittingham, Electrochem. Solid State. Lett. 3 (2000) 309.
[43] Y.J. Shin, J.P. Doumerc, P. Dordor, M. Pouchard, P. Hagenmuller, J. Solid State Chem. 107 (1993) 194.
[44] J.B. Goodenough, Phys. Rev. 100 (1955) 564.
[45] J. Kanamori, J. Appl. Phys. Supp. 31 (1960) S14.